Episodic Tremor and Slip Explained by Fluid-Enhanced Microfracturing and Sealing

Maxime Bernaudin, Frederic Gueydan

Geophysical Research Letters

RESEARCH LETTER
10.1029/2018GL077586

Key Points:
- We develop a numerical modeling to reproduce episodic tremor and slip
- Slow-slip events are modeled as transient ductile strain localization assisted by microfracturing
- Nonvolcanic tremors are triggered by transient high pore fluid pressure

Supporting Information:
- Supporting Information S1

Correspondence to:
M. Bernaudin,
maxime.bernaudin@gm.univ-montp2.fr

Citation:
Bernaudin, M., & Gueydan, F. (2018). Episodic tremor and slip explained by fluid-enhanced microfracturing and sealing. *Geophysical Research Letters*, *45*, 3471–3480. https://doi.org/10.1029/2018GL077586

Received 31 OCT 2017
Accepted 3 APR 2018
Accepted article online 12 APR 2018
Published online 23 APR 2018

Episodic Tremor and Slip Explained by Fluid-Enhanced Microfracturing and Sealing

M. Bernaudin[1] and **F. Gueydan**[1]

[1]Géosciences Montpellier, Université de Montpellier, CNRS, Montpellier, France

Abstract Episodic tremor and slow-slip events at the deep extension of plate boundary faults illuminate seismic to aseismic processes around the brittle-ductile transition. These events occur in volumes characterized by overpressurized fluids and by near failure shear stress conditions. We present a new modeling approach based on a ductile grain size-sensitive rheology with microfracturing and sealing, which provides a mechanical and field-based explanation of such phenomena. We also model pore fluid pressure variation as a function of changes in porosity/permeability and strain rate-dependent fluid pumping. The fluid-enhanced dynamic evolution of microstructures defines cycles of ductile strain localization and implies increase in pore fluid pressure. We propose that slow-slip events are ductile processes related to transient strain localization, while nonvolcanic tremor corresponds to fracturing of the whole rock at the peak of pore fluid pressure. Our model shows that the availability of fluids and the efficiency of fluid pumping control the occurrence and the P-T conditions of episodic tremor and slip.

Plain Language Summary At seismic time scales, tectonic plate boundaries are characterized by brittle-ductile rheological layering, with a frictionally locked behavior leading to earthquakes at shallow levels (0–15/30 km), a long-term aseismic ductile creep at greater depths (>40/50 km) and a seismic to aseismic transition with transient slow earthquakes in-between these two domains. Up to now, no model predicts feedback between a mixed brittle-ductile rheology and the mechanical behavior of slow earthquakes. We present here a new modeling approach based on a ductile grain size-sensitive rheology with microfracturing and sealing and pore fluid pressure variations, which provides a mechanical and field-based explanation of slow-slip events and nonvolcanic tremor. Within this approach, we model for the first time transient phenomena in a brittle-ductile material, where a local increase in pore fluid pressure can explain nonvolcanic tremor triggering. Such implications open new perspectives on the quest of geological analogs of slow earthquakes as well as on numerical modelings of the entire rheological layering of plate interface, from fast and slow earthquakes to aseismic creep.

1. Episodic Tremor and Slip Overview

At seismic time scales, tectonic plate boundaries are characterized by brittle-ductile rheological layering (Dragert et al., 2004; Wech & Creager, 2011), with a frictionally locked behavior leading to earthquakes at shallow levels (0–15/30 km) and a long-term aseismic ductile creep observed geodetically at greater depths (Figure 1a). The seismic to aseismic transition occurs at temperatures of 400 to 550°C (Peacock et al., 2011) and comprises a combination of seismic slow earthquakes (nonvolcanic tremor, NVT; Figure 1b) and aseismic slow-slip events (SSE) with variable duration from days to years (Ide et al., 2007; Obara & Kato, 2016; Rogers & Dragert, 2003). Episodic tremor and slip (ETS) is the coincidence of periodic (Obara et al., 2004) or erratic (Peterson & Christensen, 2009) short-term SSEs with synchronous NVT (Dragert et al., 2004; Obara et al., 2004; Rogers & Dragert, 2003; Shelly et al., 2006). Studies suggest that NVTs occur not only on the fault plane but also above the subduction plate interface (Obara et al., 2004; Plourde et al., 2015) and are triggered either by earthquakes (Rubinstein et al., 2007), solid earth tides (Thomas et al., 2009), and atmospheric events (Liu et al., 2009) highlighting a critically stressed system. SSEs are classically viewed as slow shear slip on frictional faults along the plate interface (Ide et al., 2007; Rubinstein et al., 2007; Shelly et al., 2006), which is related to high pore fluid pressure (Liu & Rice, 2007; Segall et al., 2010).

Various frameworks have been developed to model transient slip episodes at critically stressed conditions. Rate-and-state friction models that include a zone of low effective normal stress downdip of the seismogenic zone can produce transient slow slip along a fault plane (Liu, 2013; Liu & Rice, 2007, 2009). At those depths, however, geological data and laboratory experiments indicate that shear zone deformation occurs on

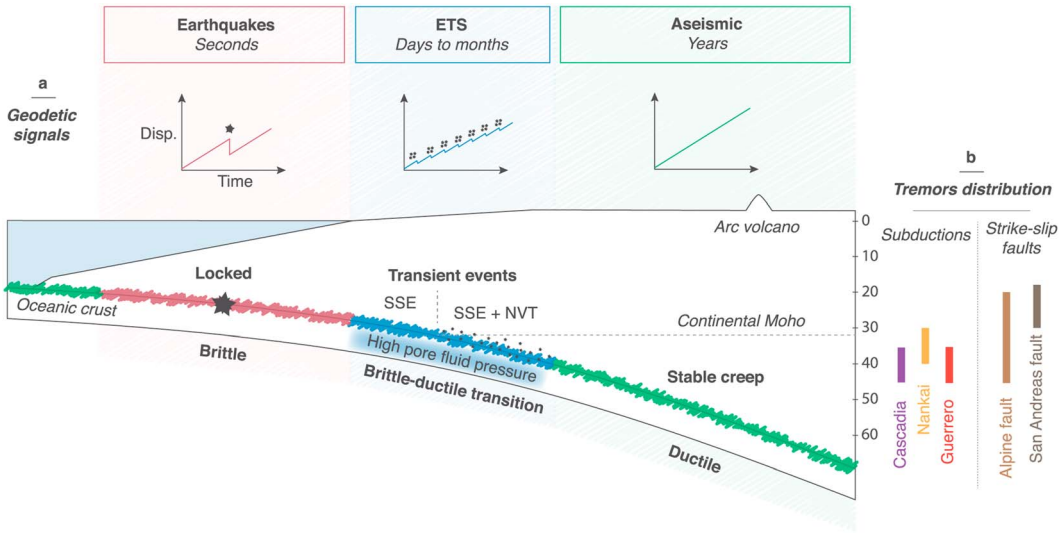

Figure 1. Different slip modes occurring along the plate interface. (a) Locked domain (red with earthquakes as black stars), transient events domain with ETS (blue with NVT as black points), and stable slip domain (green) in a subduction plate interface (modified from Peng and Gomberg, 2010). The light blue area indicates high pore fluid pressure inferred from v_P/v_S ratio studies (Audet et al., 2009; Peacock et al., 2011). Figurative displacement versus time diagram (up) for the three domains (modified from Dragert et al., 2004). (b) NVT depth locations for subduction and strike-slip plate interfaces.

kilometer-wide structures (Hayman & Lavier, 2014; Reber et al., 2015). A transition from frictional sliding to fully viscous shear with high pore fluid pressure conditions is therefore invoked to explain the location of both SSE and ETS along subduction plate interfaces (Gao & Wang, 2017). In this approach, SSEs can be modeled with a visco-elasto-plastic model by episodic fractures/slips on well-oriented strong lenses embedded in a viscous creeping material (Hayman & Lavier, 2014; Lavier et al., 2013). In a fluid-saturated fault zone, SSEs may also result from shear heating and associated fast mineralogical changes (e.g., serpentinization) that imply variations in porosity and hence pore fluid pressure (Alevizos et al., 2014). Temperature-dependent permeability reduction in the fault plane by sealing process (silica enrichment of gouge) may as well lead to differential overpressure development that controls ETS recurrence time (Audet & Bürgmann, 2014). All these previous studies highlight the importance of brittle-ductile rheology and high pore fluid pressure conditions. Up to now, no model predicts feedback between a mixed brittle-ductile rheology, SSE, and an evolving pore fluid pressure that can trigger NVT.

We develop a modeling approach that quantifies the feedback between a dynamically evolving microstructure and fluid pumping in a ductile material, which is sheared at high pore fluid pressure conditions (Figure 2). This approach is motivated by key geological observations of exhumed deep-seated centimeter-to-meter-scale shear zones deformed at 400–550°C (Figure 2a; Gueydan et al., 2003, 2017; Gueydan et al., 2004). These shear zones show typical brittle-ductile behavior with an overall ductile deformation (e.g., foliated rocks) associated with microfracturing of the strong phase grains (grain size reduction; Fagereng et al., 2014; Gueydan et al., 2003; Hayman & Lavier, 2014) (Figures 2b and 2c). This microfracturing and the development of kilometer-scale shear zones lead ultimately to mineralogical changes (e.g., metamorphic reactions) that take place at the million-year time scale (Gueydan et al., 2014) that we disregard here. At shorter timescales, ductile strain localization is often associated with porosity/permeability evolution (Simpson, 1985) related to dynamic fluid pumping (Fusseis et al., 2009; Menegon et al., 2015), which enhances sealing of the microfractures (Figure 2b). Typically, the same mineral as the fractured grain fills the microfractures during sealing, allowing the recovery of the grain (e.g., grain size increase; Figures 2b and 2c). Furthermore, fluid pumping during strain localization can trigger whole rock fracturing at near lithostatic pore fluid pressure conditions (Figure 2c). In our model, evolving microstructures correspond to microfracturing of the strong phase and subsequent sealing (Figure 2c) and leads to dynamic evolution of porosity/permeability. Numerical modeling is therefore necessary to capture the complex interplay between dynamic fluid properties and ductile transient deformation, and its potential to generate SSE and NVT.

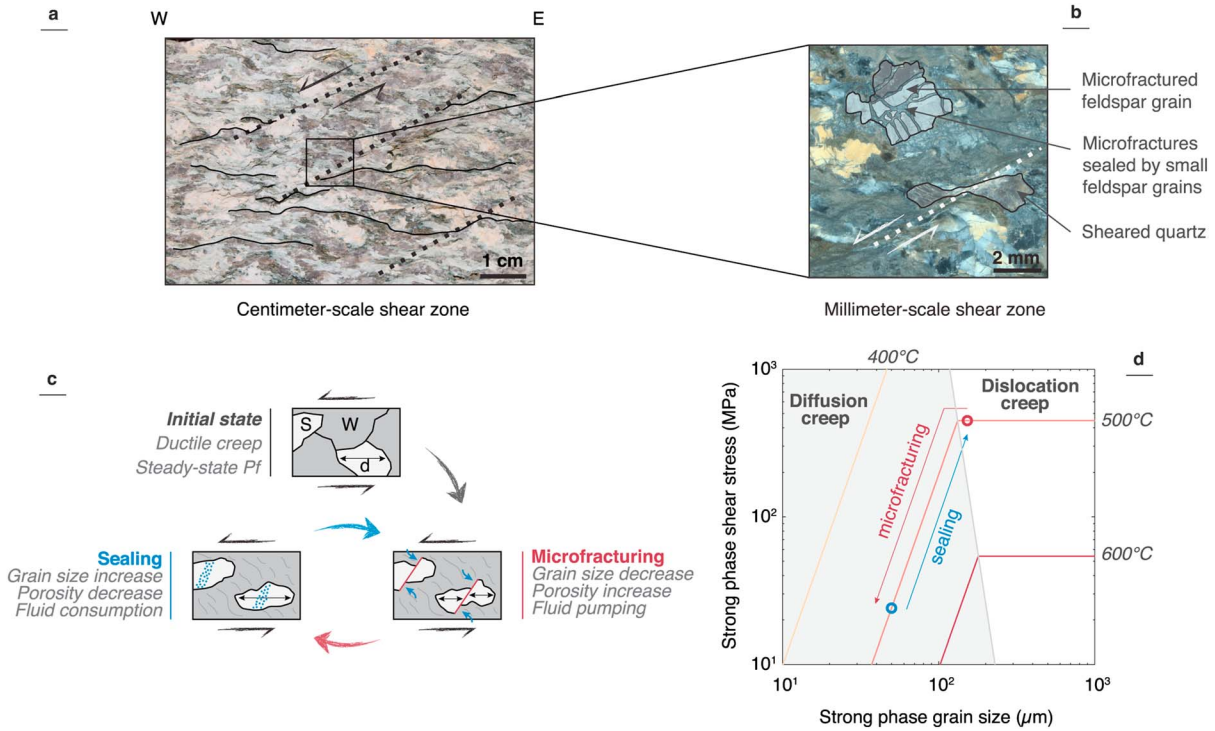

Figure 2. Key field observations used to define the grain size-sensitive rheology. (a) Centimeter-scale shear zones (black dashed lines) in foliated (thin black lines) granitic rocks from East Tenda Shear Zone (Gueydan et al., 2003, 2017; Corsica, France). (b) Zoom on associated microstructure (white dashed line) with sheared quartz and microfractures in feldspar that are sealed by small grains of feldspar. (c) Schematic description of the grain size-sensitive rheological model (with microfracturing and sealing as short-term grain size reduction and grain growth processes) with dynamic fluid properties. Initial state: Bi-phase ductile aggregate (weak phase-W is quartz; strong phase-S is feldspar). Second step: microfracturing (i.e., grain size reduction) of the strongest phase with related porosity increase and fluid pumping. Third step: sealing (i.e., grain growth) with fluid consumption and porosity decrease. (d) Deformation mechanism map for wet feldspar (Rybacki & Dresen, 2000). The grey and white areas define domains where diffusion and dislocation creep, respectively, are dominant (low and high grain size, respectively). The red (microfracturing) and blue (sealing) arrows show dynamic evolution of grain size and shear stress.

2. Rheological Model

The rheological model is described by an overall grain size-sensitive (GSS) two-phase ductile material (equation (1)) with no preexisting fractures (Figure 2c). The material consists of an aggregate of a strong phase (subscript f; feldspar) and a weak phase (subscript q; quartz), which corresponds to a continental environment (e.g., San Andreas fault or subduction interface with a continental upper plate). Other assemblages more representative of oceanic environments may be considered (e.g., plagioclase and pyroxene), but the main results described herein only require a rheological contrast between a strong and a weak mineral phase (see supporting information S1). The material shear stress (τ) is the weighted sum of the strength of the two minerals (τ_f and τ_q, respectively; equation (1); Handy, 1994; Tullis et al., 1991):

$$\tau = C_f \tau_f + C_q \tau_q, \tag{1}$$

where C_f and C_q are feldspar and quartz proportions, respectively (set here to 50% each; see supporting information S1 for other proportions). Strain rate is defined as a function of shear stress, temperature, and grain size by the combination of diffusion (GSS) and dislocation (grain size-insensitive, GSI) creep flow laws (Rybacki & Dresen, 2000; Hirth et al., 2001; equation (2)):

$$\dot{\varepsilon}_i = A_{\mathrm{GSI},i} \tau_i^{n_{GSI,i}} e^{-\frac{Q_{\mathrm{GSI},i}}{RT}} + A_{\mathrm{GSS},i} \tau_i^{n_{\mathrm{GSS},i}} d^{-p_{\mathrm{GSS},i}} e^{-\frac{Q_{\mathrm{GSS},i}}{RT}}, \tag{2}$$

where i indicates strong or weak phase, $\dot{\varepsilon}$ is the strain rate, A is a material constant, n is the stress exponent, Q is the activation energy, R is the molar gas constant, T is the absolute temperature, d is the grain size, and p is the grain size exponent (Figure 2d). Note that only dislocation creep is used for quartz. This GSS rheology allows shear stress variations as a function of grain size, where grain size decrease leads to rock weakening and grain size increase leads to rock hardening (Figure 2d).

Short-term grain size evolution (Figure 2b) is modeled by microfracturing (detected by Mohr-Coulomb criterion on the strong phase shear stress) and sealing:

$$\dot{d} = \left(\varphi_s \dot{\varepsilon} - \alpha_{\mu f}\right) d \tag{3}$$

with

$$\begin{cases} \alpha_{\mu f} = 0, & \text{if } \tau_f < \tau^y = \mu(\sigma_n - P_f) \\ \alpha_{\mu f} \neq 0, & \text{if } \tau_f \geq \tau^y = \mu(\sigma_n - P_f) \end{cases} \tag{4}$$

where φ_s stands for sealing kinematic, $\alpha_{\mu f}$ is the microfracturing kinematic, μ is the friction coefficient, σ_n is the normal stress, and P_f is the pore fluid pressure. We define microfracturing as fracturing of a single grain (Gueydan et al., 2003; Fusseis & Handy, 2008; Figure 2a). Microfracturing contributes to strain since it allows strength reduction within diffusion creep domain (Figure 2d). Short-term grain size growth (Figure 2b) corresponds to sealing and healing of microfractures (Gratier et al., 2003) and veins (Giger et al., 2007) by fluid consumption. We simplified this mechanism using a strain rate-dependent sealing process following Gratier and Gueydan (2007) (equation (3)). For this study we set sealing kinematic φ_s to 7.10^6 in order to have a characteristic time of sealing of 50 days. Note that this kinematic of sealing is a free parameter and its value controls the recurrence time of strain localization.

We express pore fluid pressure variations using Darcy's law and the fluid mass conservation (Gratier et al., 2003) leading to

$$\phi_m C \frac{\partial P_f}{\partial t} + \frac{\partial \phi_m}{\partial t} = \frac{\partial \left(K \frac{\partial P_f}{\partial x}\right)}{\partial x} + F \tag{5}$$

where ϕ_m is the mean porosity, C is the mean matrix-fluid compressibility, t is time, x is the distance across the shear zone, K is the permeability, and F is the fluid pumping parameter. We relate porosity and permeability following Skarbek and Rempel (2016):

$$K = K_0 \left(\frac{\phi}{\phi_0}\right)^{\alpha_k} \tag{6}$$

where K_0 is the permeability at a reference porosity ϕ_0 and α_k is the permeability exponent (set here to 3, see Skarbek & Rempel, 2016). Observations on midcrustal granitic shear zones show that porosity concentrates along grain boundaries and decreases with the distance to the core of the shear zone (Fusseis et al., 2009). Therefore, we assume that porosity is inversely proportional to grain size (see supporting information S2).

Finally, we model the enhancement of fluid pumping by ductile deformation as

$$\dot{F} = \varphi_F F \dot{\varepsilon} \tag{7}$$

where F is the fluid pumping and φ_F is the kinematic of the fluid pumping. The strain rate-dependent fluid pumping assumption is required to describe both strong fluid circulation in the core of the shear zone and nearly no fluid circulation at the rim. We set the kinematic of fluid pumping φ_F to 7.10^4 in order to have a characteristic time of fluid pumping of 5,000 days (~14 years). Note that a lower fluid pumping rate inhibits strain localization described below while a larger fluid pumping rate implies numerical instabilities.

3. Numerical Experiments

We perform a simple shear experiment in 1-D by numerically solving, within an implicit scheme, the mechanical equilibrium $\partial\tau/\partial y = 0$ and Darcy's law across a 10-km-thick section at given depth and temperature. Shear velocity is set at 1 cm/year. The initial grain size is randomized at 80 μm ±5%, and the initial pore fluid pressure is set at $\lambda = 0.8$ (λ is the pore fluid factor and corresponds to the ratio of pore fluid pressure to lithostatic pressure). Three types of behaviors are observed, as a function of initial temperature: (1) a fully brittle behavior at low temperature (i.e., $\tau > \tau^y$), (2) a fully ductile creep at high temperature, and (3) an overall ductile behavior at intermediate temperature (i.e., $\tau < \tau^y$) but with feldspar shear stress being greater than the yield stress ($\tau_f > \tau^y$, i.e., microfracturing of feldspar grains). The temperature window of this brittle-ductile behavior depends on the initial pore fluid pressure (equation (4)) and the selected flow laws (equation (2)). Episodic transient strain localization driven by the competition between microfracturing and sealing is detected

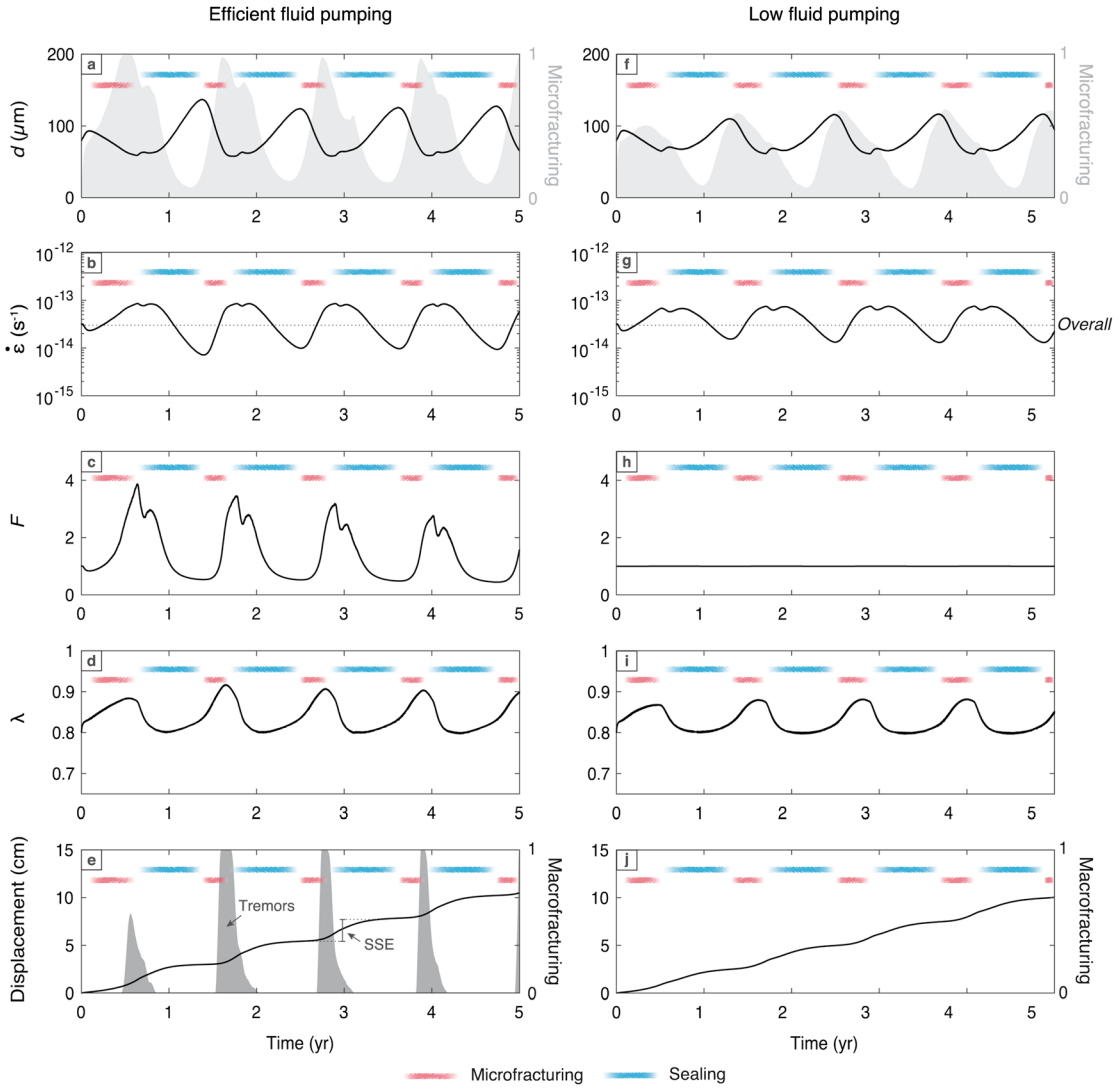

Figure 3. 1-D numerical results of transient strain localization driven by microfracturing and sealing (at 40-km depth, 500°C, and initial pore fluid factor of [λ = 0.8]). Note that all curves correspond to a mean value inside a 400-m-thick section where recorded strain localization is the highest. (a–e) A case with efficient fluid pumping. (f–j) A case with low fluid pumping. Time evolution of (a and f) feldspar grain size (with microfracturing as light shaded area), (b and g), strain rate (overall strain rate as dashed line), (c and h) fluid pumping efficiency, (d and i), pore fluid factor, and (e and j), displacement (time integral of strain rate within a 1-km-thick shear band) with macrofracturing as dark shaded area. In b and g, the imposed simple shear velocity at the boundaries yields an overall strain rate of ~3.10^{-14} s^{-1} (dashed line). The red and blue areas highlight microfracturing and sealing stages, respectively.

only for this brittle-ductile case (shown at 40 km and 500°C in Figure 3) and for high rate of sealing and fluid pumping.

Example results are shown in Figure 3 (see Figure S3 for results across shear zone). The initial grain size and strain rate involve a short episode of sealing of feldspar grains (Figures 3a and 3b), implying increase in pore fluid pressure. Subsequently, microfracturing (t = 0.1 year) leads to grain size decrease that progressively weakens the material (GSS rheology; equation (2)) and triggers the onset of strain localization (ratio of maximum strain rate over minimum strain rate; Figure 3b). The increase of strain rate enhances the fluid pumping (Figure 3c), leading to a continuous increase of pore fluid pressure (Figure 3d) that enhances microfracturing. Such behavior defines a positive feedback between microfracturing, strain localization, and fluid pumping.

Subsequently, the large values of strain rate also increase the sealing rate (equation (3)) that progressively becomes equivalent to the microfracturing rate, thus ending grain size reduction (t = 0.7 year; Figure 3a). The onset of fracture filling and fluid consumption by sealing lead to a decrease in pore fluid pressure and

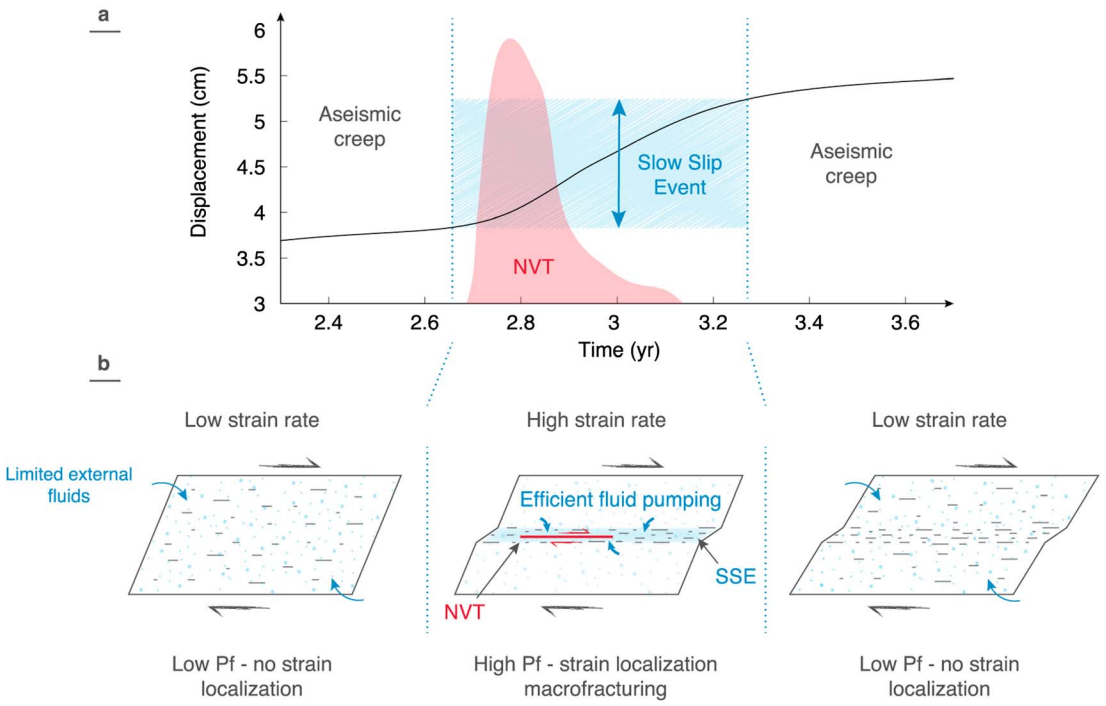

Figure 4. Short-term ductile shear zone evolution and proposed ETS triggering. (a) Modeled SSE (displacement in black curve) and NVT (macrofracturing in red shaded area) from one cycle of ductile strain localization. The blue dashed lines and shaded area delimit ETS from aseismic creep. (b) Short-term evolution of a centimeter-scale shear zone. (left) During aseismic creep, low strain rate (no strain localization). (middle) Microfracturing promotes strain rate increase. SSE occurs by ductile strain localization. The positive feedback between fluid pumping (blue) and strain localization allows high pore fluid pressure that triggers NVT. (Right) Sealing leads to the decrease of pore fluid pressure and the increase of grain size by sealing and hence to strain rate decreases and a new period of aseismic creep.

grain growth. Sealing becomes dominant over microfracturing leading to the strengthening of the material and continued pore fluid pressure decrease (t = 0.8–1 year; Figure 3d). The large increase in grain size leads to the decrease of the strain rate by at least 1 order of magnitude that drastically reduces the sealing efficiency and decrease values of porosity/permeability, which trigger pore fluid pressure increase (t = 1–1.2 years; Figure 3c). As a consequence, microfracturing becomes again dominant over sealing and these feedback loops define cycles of ductile strain localization (t = 1.4 years; Figure 3a). With moderate to low fluid pumping, strain localization cycles are still present but variations of both strain rate and pore fluid pressure are damped (Figures 3g and 3i).

4. A Mechanical Model for Episodic Tremor and Slip

This model is the first model to propose a fluid-enhanced competition between microfracturing and sealing, which defines cycles of transient strain localization associated with pore fluid pressure fluctuations. Such temporal variations of strain rate by 1 order of magnitude induce a nonuniform displacement through time with approximately 2 cm of cumulated displacement per event, within a 1-km-thick shear band (Figures 3e and 4a). We propose that these strain localization events correspond to recurring SSE. Microfracturing and sealing rates control the duration and the recurrence time of these transient events, respectively. Episodically, high pore fluid pressure sufficiently decreases Mohr-Coulomb yield stress to trigger fracturing of the whole rock (e.g., macrofracturing; Figure 3e). During SSE, these short episodes of macrofracturing are assumed to be a model proxy for NVT (Figures 4a and 4b). Maximal pore fluid pressures are reached at the maximum microfracturing activity that allows large porosity/permeability, large strain rate, and therefore large fluid pumping (Figure 3c). We therefore reproduce the ETS behavior with both episodic SSE (i.e., transient strain localization triggered by microfracturing and efficient fluid pumping; Figure 4b) and NVT (i.e., macrofracturing triggered by overpressured conditions). ETS occurrence (i.e., SSE and NVT) requires efficient fluid pumping, since no macrofracturing is detected with moderate or no fluid pumping (Figures 3h and 3j).

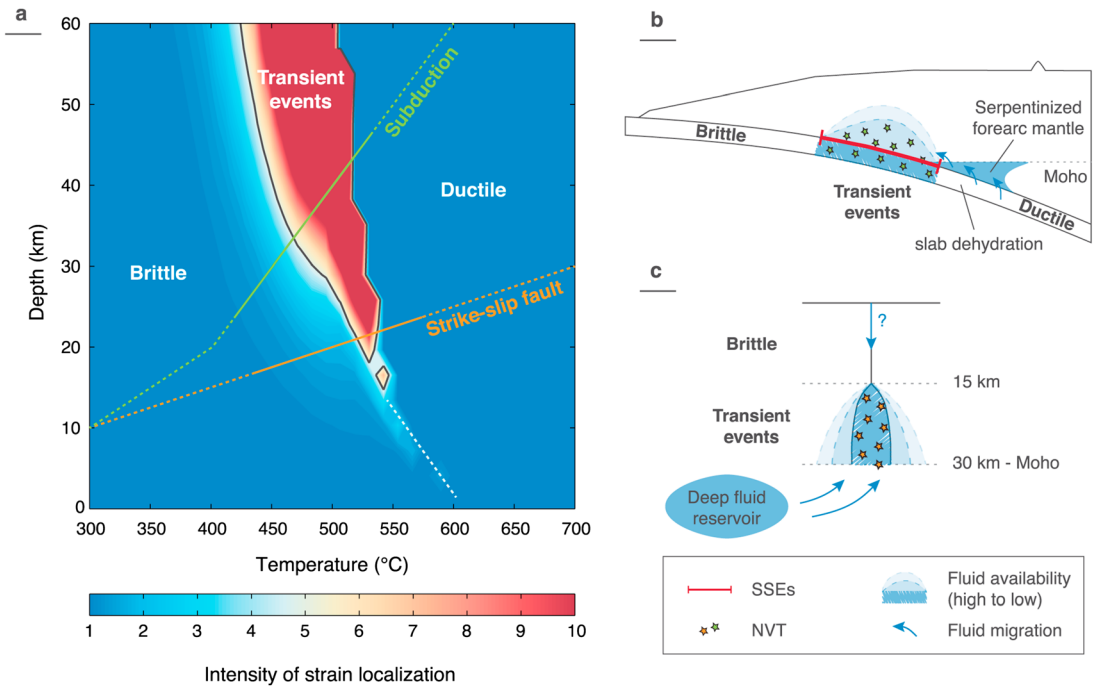

Figure 5. Modeled depth and temperature ranges for ETS in subduction and strike-slip setting. (a) Episodic tremor and slip domain (initial pore fluid factor of $\lambda = 0.8$) inferred from 400 model outputs. The blue-to-red color scale describes the intensity of strain localization (ratio of maximum strain rate over minimum strain rate at a given time) and high pore fluid pressure inferred from our models. The thin dark line highlights domain of ETS prediction. The green and orange lines correspond to subduction (Cascadia, Nankai, and Guerrero) and strike-slip faults (San Andreas and Alpine faults) mean geotherm respectively. (b and c) Conceptual model of ETS occurrence related to fluid sources in subduction zone (b) and strike-slip faults (c).

5. ETS Triggering in Subduction and Strike-Slip Fault

Our model allows identifying the depth-temperature ranges at which SSEs and associated NVT can occur (Figure 5a), which are bounded by fully brittle behavior at low temperature (<400°C) and ductile creep at high temperature (>600°C). Only intermediate temperatures (400°C < T < 600°C) and initial high pore fluid pressure ($\lambda > 0.70$; see supporting information S4) predict ETS behavior. ETS are rather pressure-insensitive since they can occur from 15-km to more than 60-km depth. The temperature window (here between 450 and 550°C) is controlled by the rheological parameters. Using a weaker feldspar rheology or a larger proportion of quartz will decrease the lower temperature limit of ETS to ~400°C.

In natural subduction zone examples, SSEs occur between 20- and 60-km depths (e.g., Cascadia, Guerrero, and Nankai; see Brown et al., 2009; Kostoglodov et al., 2010; Wada et al., 2008; Yoshioka et al., 2008) and the NVT are located in a more restricted depth ranges (30–45 km; Figure 5a) at an estimated temperature of 400–500°C (Manea et al., 2004; Peacock et al., 2002). In strike-slip fault settings (e.g., San Andreas fault and Alpine fault; see Shelly & Hardebeck, 2010; Wech et al., 2012) NVT are recorded between 15- and 30-km depth, corresponding to a temperature range of 500–700°C (Sass et al., 1997; Toy et al., 2010; Figure 5a). Only NVT can be discussed for strike-slip faults since concurrent SSEs are not yet resolved with current data (Rubinstein et al., 2010). Our model results are remarkably consistent with these data (Figure 5a) since they imply ETS occurrence at 30–45 km and 400–500°C in a subduction context (cold geotherm) and at 15–30 km and around 500°C in strike-slip fault context (normal to hot geotherm). Note that the modeled depth and temperature ranges of ETS will depend on the selected material (continental or oceanic crust), the initial pore fluid pressure, and the fluid pumping efficiency (see supporting information S4).

6. Discussion and Conclusions

At subduction zones, SSEs and NVT association is now well confirmed on the deep portions of subduction faults (Obara & Kato, 2016; Shelly et al., 2007), where high pore fluid pressure is also well documented

(Audet et al., 2009; Peacock et al., 2011) with fluids coming from slab dehydration and de-serpentinization (Fagereng & Diener, 2011; Figure 5b). These fluids are required in our model to trigger ETS (Figure 3) since with moderate incoming fluids we predict only SSEs with no NVT. In some subduction systems, SSEs without NVT can therefore be explained by the presence of low to moderate amounts of fluids (Ide, 2012; Wech & Bartlow, 2014; Figures 3f–3j). When fluids migrate within the overriding plate, NVT can be likely triggered by SSEs in the whole domain from the fault plane to shallower depths (Peterson & Christensen, 2009; Figure 5b).

In a strike-slip fault context, SSEs remain to be accurately identified (Brenguier et al., 2008; Johnson et al., 2013). However, precise NVT source location on the San Andreas fault system suggests that they occur below the fault plane and extend at least to the base of the crust (Shelly, 2010; Shelly & Hardebeck, 2010). NVT are always recorded in the presence of near-lithostatic pore fluid pressure conditions (Thomas et al., 2009). Fluids necessary to trigger our ETS mechanism can originate from adjacent rocks in the midlower crust (dehydration of serpentinites; Becken et al., 2011) or perhaps from transient sources of meteoric fluids during fault rupture (Figure 5c).

The recurrence time of SSEs and ETS spans from months to years in natural cases (Obara & Kato, 2016), and mechanism explaining this diversity is still elusive. Audet and Bürgmann (2014) propose that permeability reduction by silica enrichment of fault gouge controls the recurrence time of ETS. In our model we propose that this recurrence time is related to the rate of sealing, which also implies a permeability reduction. This sealing process is modeled by a single parameter that integrates complex processes such as transport and precipitation or facture healing (Gratier et al., 2003). Further field and geophysical observations combined with laboratory experiments are required to better constrain sealing/healing processes at depth, especially their short-term kinetics (Fisher & Brantley, 2014) and temperature dependency (Giger et al., 2007).

In conclusion, our model successfully reproduces the entire complex rheological layering along the subduction plate interface, including the locked, transient, and aseismic creep domains. In particular, we model for the first time transient phenomena in a brittle-ductile material, thus providing a dynamic framework expanding on the work of Gao and Wang (2017). We also model local increase in pore fluid pressure that likely explains NVT triggering.

Acknowledgments
We thank S. Mazzotti for valuable discussions and constructive comments on the manuscript. Both M. B. and F. G. contributed to the model development, the interpretations, and preparation of the final manuscript. The authors declare no competing financial interests. Numerical code to reproduce simulation results is available upon request. Input parameters are available on supporting information.

References

Alevizos, S., Poulet, T., & Veveakis, E. (2014). Thermo-poro-mechanics of chemically active creeping faults. 1: Theory and steady state considerations. *Journal of Geophysical Research: Solid Earth*, *119*, 4558–4582. https://doi.org/10.1002/2013JB010070

Audet, P., Bostock, M. G., Christensen, N. I., & Peacock, S. M. (2009). Seismic evidence for overpressured subducted oceanic crust and megathrust fault sealing. *Nature*, *457*(7225), 76–78. https://doi.org/10.1038/nature07650

Audet, P., & Bürgmann, R. (2014). Possible control of subduction zone slow-earthquake periodicity by silica enrichment. *Nature*, *510*(7505), 389–392. https://doi.org/10.1038/nature13391

Becken, M., Ritter, O., Bedrosian, P. A., & Weckmann, U. (2011). Correlation between deep fluids, tremor and creep along the central San Andreas fault. *Nature*, *480*(7375), 87–90. https://doi.org/10.1038/nature10609

Brenguier, F., Campillo, M., Hadziioannou, C., Shapiro, N. M., Nadeau, R. M., & Larose, E. (2008). Postseismic relaxation along the San Andreas fault at Parkfield from continuous seismological observations. *Science*, *321*(5895), 1478–1481. https://doi.org/10.1126/science.1160943

Brown, J. R., Beroza, G. C., Ide, S., Ohta, K., Shelly, D. R., Schwartz, S. Y., et al. (2009). Deep low-frequency earthquakes in tremor localize to the plate interface in multiple subduction zones. *Geophysical Research Letters*, *36*, L19306. https://doi.org/10.1029/2009GL040027

Dragert, H., Wang, K., & Rogers, G. (2004). Geodetic and seismic signatures of episodic tremor and slip in the northern Cascadia subduction zone. *Earth, Planets and Space*, *56*(12), 1143–1150. https://doi.org/10.1186/BF03353333

Fagereng, Å., & Diener, J. F. (2011). Non-volcanic tremor and discontinuous slab dehydration. *Geophysical Research Letters*, *38*, L15302. https://doi.org/10.1029/2011GL048214

Fagereng, Å., Hillary, G. W., & Diener, J. F. (2014). Brittle-viscous deformation, slow slip, and tremor. *Geophysical Research Letters*, *41*, 4159–4167. https://doi.org/10.1002/2014GL060433

Fisher, D. M., & Brantley, S. L. (2014). The role of silica redistribution in the evolution of slip instabilities along subduction interfaces: Constraints from the Kodiak accretionary complex, Alaska. *Journal of Structural Geology*, *69*, 395–414. https://doi.org/10.1016/j.jsg.2014.03.010

Fusseis, F., & Handy, M. R. (2008). Micromechanisms of shear zone propagation at the brittle–viscous transition. *Journal of Structural Geology*, *30*(10), 1242–1253. https://doi.org/10.1016/j.jsg.2008.06.005

Fusseis, F., Regenauer-Lieb, K., Liu, J., Hough, R. M., & De Carlo, F. (2009). Creep cavitation can establish a dynamic granular fluid pump in ductile shear zones. *Nature*, *459*(7249), 974–977. https://doi.org/10.1038/nature08051

Gao, X., & Wang, K. (2017). Rheological separation of the megathrust seismogenic zone and episodic tremor and slip. *Nature*, *543*(7645), 416–419. https://doi.org/10.1038/nature21389

Giger, S. B., Tenthorey, E., Cox, S. F., Gerald, F., & John, D. (2007). Permeability evolution in quartz fault gouges under hydrothermal conditions. *Journal of Geophysical Research*, *112*, B07202. https://doi.org/10.1029/2006JB004828

Gratier, J. P., Favreau, P., & Renard, F. (2003). Modeling fluid transfer along California faults when integrating pressure solution crack sealing and compaction processes. *Journal of Geophysical Research*, *108*(B2), 2104. https://doi.org/10.1029/2001JB000380

Gratier, J. P., & Gueydan, F. (2007). Effect of fracturing and fluid–rock interaction on seismic cycles. *Tectonic Faults: Agents of Change on a Dynamic Earth*, *95*, 319e356.

Gueydan, F., Brun, J. P., Phillippon, M., & Noury, M. (2017). Sequential extension as a record of Corsica Rotation during Apennines slab roll-back. *Tectonophysics*, *710*, 149–161.
Gueydan, F., Leroy, Y. M., & Jolivet, L. (2004). Mechanics of low-angle extensional shear zones at the brittle-ductile transition. *Journal of Geophysical Research*, *109*, B12407. https://doi.org/10.1029/2003JB002806
Gueydan, F., Leroy, Y. M., Jolivet, L., & Agard, P. (2003). Analysis of continental midcrustal strain localization induced by microfracturing and reaction-softening. *Journal of Geophysical Research*, *108*(B2), 2064. https://doi.org/10.1029/2001JB000611
Gueydan, F., Précigout, J., & Montesi, L. G. (2014). Strain weakening enables continental plate tectonics. *Tectonophysics*, *631*, 189–196. https://doi.org/10.1016/j.tecto.2014.02.005
Handy, M. R. (1994). Flow laws for rocks containing two non-linear viscous phases: A phenomenological approach. *Journal of Structural Geology*, *16*(3), 287–301. https://doi.org/10.1016/0191-8141(94)90035-3
Hayman, N. W., & Lavier, L. L. (2014). The geologic record of deep episodic tremor and slip. *Geology*, *42*(3), 195–198. https://doi.org/10.1130/G34990.1
Hirth, G., Teyssier, C., & Dunlap, J. W. (2001). An evaluation of quartzite flow laws based on comparisons between experimentally and naturally deformed rocks. *International Journal of Earth Sciences*, *90*(1), 77–87. https://doi.org/10.1007/s005310000152
Ide, S. (2012). Variety and spatial heterogeneity of tectonic tremor worldwide. *Journal of Geophysical Research*, *117*, B03302. https://doi.org/10.1029/2011JB008840
Ide, S., Beroza, G. C., Shelly, D. R., & Uchide, T. (2007). A scaling law for slow earthquakes. *Nature*, *447*(7140), 76–79. https://doi.org/10.1038/nature05780
Johnson, K. M., Shelly, D. R., & Bradley, A. M. (2013). Simulations of tremor-related creep reveal a weak crustal root of the San Andreas fault. *Geophysical Research Letters*, *40*, 1300–1305. https://doi.org/10.1002/grl.50216
Kostoglodov, V., Husker, A., Shapiro, N. M., Payero, J. S., Campillo, M., Cotte, N., & Clayton, R. (2010). The 2006 slow slip event and nonvolcanic tremor in the Mexican subduction zone. *Geophysical Research Letters*, *37*, L24301. https://doi.org/10.1029/2010GL045424
Lavier, L. L., Bennett, R. A., & Duddu, R. (2013). Creep events at the brittle ductile transition. *Geochemistry, Geophysics, Geosystems*, *14*(9), 3334–3351. https://doi.org/10.1002/ggge.20178
Liu, C., Linde, A. T., & Sacks, I. S. (2009). Slow earthquakes triggered by typhoons. *Nature*, *459*(7248), 833–836. https://doi.org/10.1038/nature08042
Liu, Y. (2013). Numerical simulations on megathrust rupture stabilized under strong dilatancy strengthening in slow slip region. *Geophysical Research Letters*, *40*, 1311–1316. https://doi.org/10.1002/grl.50298
Liu, Y., & Rice, J. R. (2007). Spontaneous and triggered aseismic deformation transients in a subduction fault model. *Journal of Geophysical Research*, *112*, B09404. https://doi.org/10.1029/2007JB004930
Liu, Y., & Rice, J. R. (2009). Slow slip predictions based on granite and gabbro friction data compared to GPS measurements in northern Cascadia. *Journal of Geophysical Research*, *114*, B09407. https://doi.org/10.1029/2008JB006142
Manea, V. C., Manea, M., Kostoglodov, V., Currie, C. A., & Sewell, G. (2004). Thermal structure, coupling and metamorphism in the Mexican subduction zone beneath Guerrero. *Geophysical Journal International*, *158*(2), 775–784. https://doi.org/10.1111/j.1365-246X.2004.02325.x
Menegon, L., Fusseis, F., Stünitz, H., & Xiao, X. (2015). Creep cavitation bands control porosity and fluid flow in lower crustal shear zones. *Geology*, *43*(3), 227–230. https://doi.org/10.1130/G36307.1
Obara, K., Hirose, H., Yamamizu, F., & Kasahara, K. (2004). Episodic slow slip events accompanied by non-volcanic tremors in southwest Japan subduction zone. *Geophysical Research Letters*, *31*, L23602. https://doi.org/10.1029/2004GL020848
Obara, K., & Kato, A. (2016). Connecting slow earthquakes to huge earthquakes. *Science*, *353*(6296), 253–257. https://doi.org/10.1126/science.aaf1512
Peacock, S. M., Christensen, N. I., Bostock, M. G., & Audet, P. (2011). High pore pressures and porosity at 35 km depth in the Cascadia subduction zone. *Geology*, *39*(5), 471–474. https://doi.org/10.1130/G31649.1
Peacock, S. M., Wang, K., & McMahon, A. M. (2002). Thermal structure and metamorphism of subducting oceanic crust: Insight into Cascadia intraslab earthquakes. In S. Kirby, K. Wang, & S. Dunlop (Eds.), *The Cascadia Subduction Zone and Related Subduction Systems: Seismic Structure, Intraslab Earthquakes and Processes, and Earthquake Hazards* (U.S. Geol. Surv. Open File Rep., 02-328, pp. 123–126). https://pubs.usgs.gov/of/2002/0328/
Peng, Z., & Gomberg, J. (2010). An integrated perspective of the continuum between earthquakes and slow-slip phenomena. *Nature Geoscience*, *3*(9), 599–607. https://doi.org/10.1038/ngeo940
Peterson, C. L., & Christensen, D. H. (2009). Possible relationship between nonvolcanic tremor and the 1998–2001 slow slip event, south central Alaska. *Journal of Geophysical Research*, *114*, B06302. https://doi.org/10.1029/2008JB006096
Plourde, A. P., Bostock, M. G., Audet, P., & Thomas, A. M. (2015). Low-frequency earthquakes at the southern Cascadia margin. *Geophysical Research Letters*, *42*, 4849–4855. https://doi.org/10.1002/2015GL064363
Reber, J. E., Lavier, L. L., & Hayman, N. W. (2015). Experimental demonstration of a semi-brittle origin for crustal strain transients. *Nature Geoscience*, *8*(9), 712–715. https://doi.org/10.1038/ngeo2496
Rogers, G., & Dragert, H. (2003). Episodic tremor and slip on the Cascadia subduction zone: The chatter of silent slip. *Science*, *300*(5627), 1942–1943. https://doi.org/10.1126/science.1084783
Rubinstein, J. L., Shelly, D. R., & Ellsworth, W. L. (2010). Non-volcanic tremor: A window into the roots of fault zones. In S. Cloetingh & J. Negendank (Eds.), *New Frontiers in Integrated Solid Earth Sciences* (pp. 287–314). New York: Springer. https://doi.org/10.1007/978-90-481-2737-5_8
Rubinstein, J. L., Vidale, J. E., Gomberg, J., Bodin, P., Creager, K. C., & Malone, S. D. (2007). Non-volcanic tremor driven by large transient shear stresses. *Nature*, *448*(7153), 579–582. https://doi.org/10.1038/nature06017
Rybacki, E., & Dresen, G. (2000). Dislocation and diffusion creep of synthetic anorthite aggregates. *Journal of Geophysical Research*, *105*(B11), 26,017–26,036. https://doi.org/10.1029/2000JB900223
Sass, J. H., Williams, C. F., Lachenbruch, A. H., Galanis, S. P., & Grubb, F. V. (1997). Thermal regime of the San Andreas fault near Parkfield, California. *Journal of Geophysical Research*, *102*(B12), 27,575–27,585. https://doi.org/10.1029/97JB02350-B
Segall, P., Rubin, A. M., Bradley, A. M., & Rice, J. R. (2010). Dilatant strengthening as a mechanism for slow slip events. *Journal of Geophysical Research*, *115*, B12305. https://doi.org/10.1029/2010JB007449
Shelly, D. R. (2010). Periodic, chaotic, and doubled earthquake recurrence intervals on the deep San Andreas fault. *Science*, *328*(5984), 1385–1388. https://doi.org/10.1126/science.1189741
Shelly, D. R., Beroza, G. C., & Ide, S. (2007). Non-volcanic tremor and low-frequency earthquake swarms. *Nature*, *446*(7133), 305–307. https://doi.org/10.1038/nature05666
Shelly, D. R., Beroza, G. C., Ide, S., & Nakamula, S. (2006). Low-frequency earthquakes in Shikoku, Japan, and their relationship to episodic tremor and slip. *Nature*, *442*(7099), 188–191. https://doi.org/10.1038/nature04931

Shelly, D. R., & Hardebeck, J. L. (2010). Precise tremor source locations and amplitude variations along the lower-crustal central San Andreas fault. *Geophysical Research Letters*, *37*, L14301. https://doi.org/10.1029/2010GL043672

Simpson, C. (1985). Deformation of granitic rocks across the brittle-ductile transition. *Journal of Structural Geology*, *7*(5), 503–511. https://doi.org/10.1016/0191-8141(85)90023-9

Skarbek, R. M., & Rempel, A. W. (2016). Dehydration-induced porosity waves and episodic tremor and slip. *Geochemistry, Geophysics, Geosystems*, *17*(2), 442–469. https://doi.org/10.1002/2015GC006155

Thomas, A. M., Nadeau, R. M., & Bürgmann, R. (2009). Tremor-tide correlations and near-lithostatic pore pressure on the deep San Andreas fault. *Nature*, *462*(7276), 1048–1051. https://doi.org/10.1038/nature08654

Toy, V. G., Craw, D., Cooper, A. F., & Norris, R. J. (2010). Thermal regime in the central Alpine fault zone, New Zealand: Constraints from microstructures, biotite chemistry and fluid inclusion data. *Tectonophysics*, *485*(1-4), 178–192. https://doi.org/10.1016/j.tecto.2009.12.013

Tullis, T. E., Horowitz, F. G., & Tullis, J. (1991). Flow laws of polyphase aggregates from end-member flow laws. *Journal of Geophysical Research*, *96*(B5), 8081–8096. https://doi.org/10.1029/90JB02491

Wada, I., Wang, K., He, J., & Hyndman, R. D. (2008). Weakening of the subduction interface and its effects on surface heat flow, slab dehydration, and mantle wedge serpentinization. *Journal of Geophysical Research*, *113*, B04402. https://doi.org/10.1029/2007JB005190

Wech, A. G., & Bartlow, N. M. (2014). Slip rate and tremor genesis in Cascadia. *Geophysical Research Letters*, *41*(2), 392–398. https://doi.org/10.1002/2013GL058607

Wech, A. G., Boese, C. M., Stern, T. A., & Townend, J. (2012). Tectonic tremor and deep slow slip on the Alpine fault. *Geophysical Research Letters*, *39*, L10303. https://doi.org/10.1029/2012GL051751

Wech, A. G., & Creager, K. C. (2011). A continuum of stress, strength and slip in the Cascadia subduction zone. *Nature Geoscience*, *4*(9), 624–628. https://doi.org/10.1038/ngeo1215

Yoshioka, S., Toda, M., & Nakajima, J. (2008). Regionality of deep low-frequency earthquakes associated with subduction of the Philippine Sea plate along the Nankai Trough, southwest Japan. *Earth and Planetary Science Letters*, *272*(1-2), 189–198. https://doi.org/10.1016/j.epsl.2008.04.039